Ms. for *Inorganic Chemistry* (ARTICLE, ms. ID ic-2016-01427e.R1)

2-(Methylamido)pyridine–Borane: A Tripod κ^3*N,H,H*-Ligand in Trigonal Bipyramidal Rhodium(I) and Iridium(I) Complexes with an Asymmetric Coordination of its BH_3 Group

Javier Brugos,[†] Javier A. Cabeza,*[†] Pablo García-Álvarez,[†] Alan R. Kennedy,[‡]
Enrique Pérez-Carreño,[§] and Juan F. Van der Maelen[§]

[†]Departamento de Química Orgánica e Inorgánica-IUQOEM, Centro de Innovación en Química Avanzada (ORFEO-CINQA), Universidad de Oviedo-CSIC, E-33071 Oviedo, Spain

[‡]WestCHEM, Department of Pure and Applied Chemistry, University of Strathclyde, Glasgow, G1 1XL, UK

[§]Departamento de Química Física y Analítica, Universidad de Oviedo, E-33071 Oviedo, Spain

*E-mail: jac@uniovi.es (J.A.C.)

ABSTRACT: The complexes [M(κ^3*N*,*H*,*H*-mapyBH$_3$)(cod)] (M = Rh, Ir; HmapyBH$_3$ = 2-(methylamino)pyridine–borane; cod = 1,5-cyclooctadiene), which contain a novel anionic tripod ligand coordinated to the metal atom through the amido N atom and through two H atoms of the BH$_3$ group, have been prepared by treating the corresponding [M$_2$(μ-Cl)$_2$(cod)$_2$] (M = Rh, Ir) precursor with K[mapyBH$_3$]. X-ray diffraction studies and a theoretical QTAIM analysis of their electron density have confirmed that the metal atoms of both complexes are in a very distorted trigonal bipyramidal coordination environment, in which two equatorial sites are asymmetrically spanned by the H–B–H fragment. While both 3c–2e BH–M interactions are more κ^1*H* (terminal sigma coordination of the B–H bond) than κ^2*H,B* (agostic-type coordination of the B–H bond), one BH–M interaction is more agostic than the other and this difference is more marked in the iridium complex than in the rhodium one. This asymmetry is not evident in solution, where the cod ligand and the BH$_3$ group of these molecules participate in two concurrent dynamic processes of low activation energies (VT-NMR and DFT studies), namely, a rotation of the cod ligand that interchanges its two alkene fragments (through a square pyramidal transition state) and a rotation of the BH$_3$ group about the B–N bond that equilibrates the three B–H bonds (through a square planar transition state). While the cod rotation has similar activation energy in **2** and **3**, the barrier to the BH$_3$ group rotation is higher in the iridium complex than in the rhodium one.

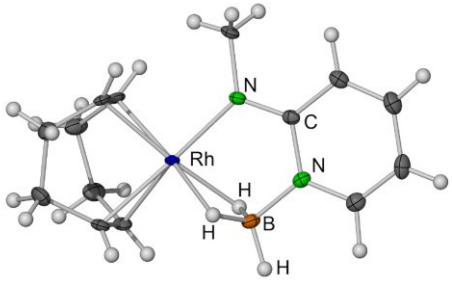

(Abstract Figure)

INTRODUCTION

The increasing interest in the use of amine–boranes ($H_2RN–BH_2R'$; R, R' = H, alkyl, aryl) as molecular systems for hydrogen storage and transportation[1] and the discovery that transition-metal complexes can promote their dehydrogenation[2,3] to give H_2 (or the transfer of H_2 to other molecules) have recently boosted the study of their coordination chemistry[2–5] and also that of aminoboranes (HRN–BHR'; R, R' = H, alkyl, aryl),[5,6] which are intermediates in the dehydrogenation of amine–boranes. In all these complexes, the ligand is attached to the metal atom, almost exclusively, through one or two of the BH groups (sigma complexes[7]), involving either κ^2*H,B* (both atoms of the BH group interact with the metal) or κ^1*H* (only the H atom of the BH group is attached to the metal) interactions. In any case, these borane–metal interactions are weak.

Some Lewis base–BH_3 adducts other than amine–boranes and aminoboranes in which their Lewis base part is also coordinable have also been recently used as ligands in transition-metal complexes (Figure 1). They are borane adducts of thiolates,[8] selenolates,[8] telurolates,[8] dithiolates,[9] pyrazolates,[10] bezothiazolate,[8] bezothiazol-2-thiolate,[8] and diphosphanes.[11] Some complexes of this type derived from substituted boranes (BH_2R and BHR_2) and appropriate Lewis bases are also known.[8,12] In some cases, the possible hemilabile character of these ligands has been verified.[11c,d,12l]

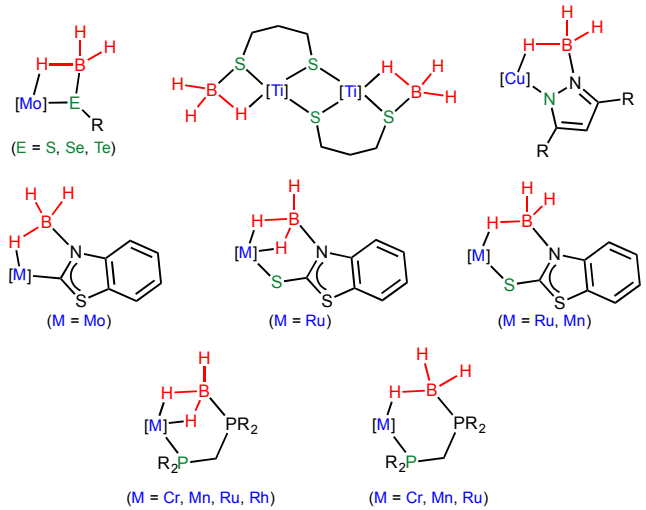

Figure 1. Examples of transition-metal complexes containing Lewis base–borane adducts as ligands that are coordinated through one or two of their BH groups and through an additional donor atom (references are given in the text).

With the objective of preparing new rhodium(I) and iridium(I) complexes containing new hemilabile ligands for subsequent catalytic investigations, we decided to use 2-(methylamino)pyridine–borane, hereafter abbreviated as $HmapyBH_3$ (**1**), as (precursor of) the hemilabile ligand because (a) it

had been previously reported that the BH_3 group of 2-aminopyridine–borane is attached to the pyridine N atom[13] and, thus, the dehydrogenation that occurs in amine–boranes is disfavored in this case, (b) an easy deprotonation of its N–H group could convert it into an unprecedented anionic ligand, namely, $[mapyBH_3]^-$, and (c) its N-methyl group would allow an easy monitoring of the reactions by ^1H NMR.

We now report the successful syntheses of the neutral rhodium(I) and iridium(I) complexes [M(κ^3*N*,*H*,*H*-mapyBH_3)(cod)] (M = Rh (**2**), Ir (**3**); cod = 1,5-cyclooctadiene). X-ray diffraction (XRD) and theoretical electron density studies, using the Quantum Theory of Atoms in Molecules (QTAIM), have confirmed that the metal atoms of both complexes are in a very distorted trigonal bipyramidal coordination environment, in which two equatorial sites are asymmetrically spanned by the BH_3 group. Interestingly, while both BH–M interactions are more terminal sigma (κ^1*H*) than agostic-type (κ^2*H,B*), one BH–M interaction is more agostic than the other and this difference is more marked in the iridium complex than in the rhodium one. Both compounds are fluxional in solution and two concurrent dynamic processes of low activation energies, involving the cod ligand and the BH_3 group of these molecules, have been identified by VT-NMR and DFT studies.

Three complexes with a structure related to that of **2** and **3** have been previously reported (Figure 2). They all are trigonal bipyramidal cationic rhodium(I) complexes that have a bis(amine–borane) (**A**[4c]) or a diphosphane–borane (**B**[11a] and **C**[11b]) as borane-containing ligands. However, in the three cases, due to lack of theoretical studies, an asymmetric coordination of the BH_3 group to the Rh atom was not recognized (and therefore it was not mentioned in the corresponding publication) despite two slightly different Rh–HB distances involving the chelating BH_3 group were observed by XRD.

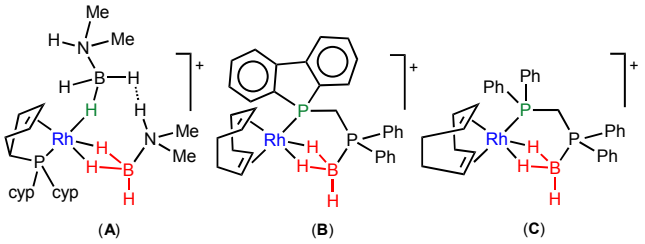

Figure 2. Previous examples of transition-metal complexes in which the coordination geometry around their metal atom is similar to that of compounds **2** and **3** (cyp = cyclopentyl; references are given in the text).

Therefore, the present work is the first one to recognize, describe, and study an asymmetric chelating coordination of the BH_2 fragment of a BH_3 group.

RESULTS AND DISCUSSION

The new aminopyridine-borane adduct HmapyBH$_3$ (**1**) was straightforwardly prepared in high yield by treating 2-(methylamino)pyridine (Hmapy) with BH$_3$·THF. Its ^{1}H and ^{11}B NMR spectra clearly show that the NH and NMe protons are not coupled to the B atom, confirming the attachment of the BH$_3$ group to the pyridine N atom, as has been previously proposed for other aminopyridine-borane adducts.[13]

Deprotonation of HmapyBH$_3$ (**1**) with K[N(SiMe$_3$)$_2$] and subsequent treatment of the resulting anion with [M$_2$(μ-Cl)$_2$(cod)$_2$] (1:0.5 mol ratio) led to the mononuclear derivatives [M(κ^3*N*,*H*,*H*-mapyBH$_3$)(cod)] (M = Rh (**2**), Ir (**3**); Scheme 1).

Scheme 1. Synthesis of Complexes 2 and 3

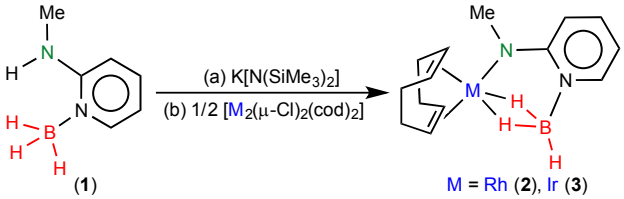

The solid-state molecular structures of **2** and **3** (Figure 3, Table 1) were determined by X-ray diffraction (XRD). Both structure determinations allowed the location and refinement of all the H atoms associated with the BH$_3$ groups. Both compounds are almost isostructural. In both cases, the metal atom (M1) is bonded to the methylamido N atom (N2), to the olefinic C atoms of the cod ligand (C1, C2, C5 and C6) and to two H atoms (H200 and H300) of the BH$_3$ group, which is also attached to the pyridine N atom (N1) through the B atom (B1). Overall, the coordination geometry around the metal atoms can be described as very distorted trigonal bipyramidal, with M1, H200, H300, C5, and C6 in the equatorial plane, the distortion being mainly caused by the narrow H200–M1–H300 angle, 62(2)º in **2** and 70(3)º in **3**.

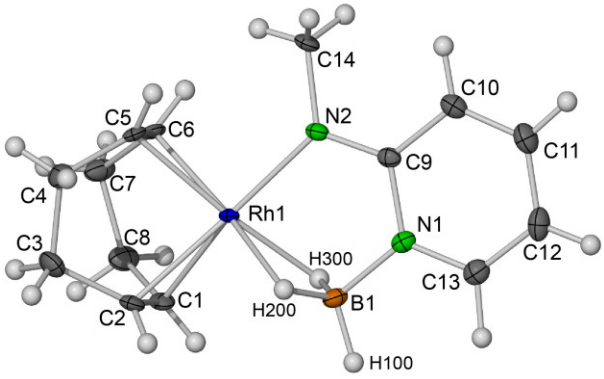

Figure 3. XRD molecular structure of **2** (50 % displacement ellipsoids). The XRD molecular structure of **3** (M = Ir) is very similar to that of **2**. Selected interatomic distances and angles in **2** and **3** are given in Table 1.

Table 1. Selected Interatomic Distances (Å) and Angles (°) in 2 and 3

Atoms	M = Rh (**2**)	M = Ir (**3**)
M1···B1	2.257(4)	2.218(4)
M1−C1	2.161(3)	2.138(4)
M1−C2	2.152(3)	2.141(4)
M1−C5	2.113(3)	2.116(4)
M1−C6	2.104(3)	2.105(4)
M1−N2	2.069(3)	2.054(4)
M1−H200	1.95(4)	1.93(6)
M1−H300	1.94(3)	1.89(5)
B1−N1	1.525(5)	1.519(6)
B1−H100	1.09(4)	1.08(5)
B1−H200	1.18(4)	1.33(6)
B1−H300	1.17(4)	1.26(6)
C1−C2	1.392(5)	1.406(7)
C5−C6	1.428(6)	1.435(7)
H200–M1–H300	62(2)	70(3)
M–H200–B1	89(3)	84(3)
M–H300–B1	90(2)	87(3)
H200–B1–H300	116(3)	116(4)

In both complexes, the M1–C1 and M1–C2 distances are *ca.* 0.05 Å longer than the M1–C5 and M1–C6 distances (Table 1). This fact may be a consequence of a different *trans* influence of the amido and BH_2 fragments, as has been claimed for the structure of complex **B** (Figure 2),[11a] but it may also be related to the axial *versus* equatorial coordination of the cod olefinic atoms, because, in homoleptic trigonal bipyramidal AB_5 species, the $A–B_{ax}$ lengths are longer than the corresponding $A–B_{eq}$ lengths.[14]

A careful analysis of the interatomic distances and angles involving the atoms of the BH_3 group and the corresponding metal atom revealed that the metrics of M1–H200–B1 and M1–H300–B1 interactions, although they are similar in the Rh complex **2**, they seem to be slightly different in the Ir complex **3** because the differences are near the limit of the experimental error. Thus, while the Rh1–H200 and Rh1–H300 distances are 1.95(4) and 1.94(3) Å, respectively, the Ir1–H200 and Ir1–H300 distances are 1.93(6) and 1.89(5) Å, respectively, and while the Rh1–H200–B1 and Rh1–H300–B1 angles are 89(3)° and 90(2)°, respectively, the Ir1–H200–B1 and Ir1–H300–B1 angles are 84(3)° and 87(3)°, respectively. In addition, the M1···B1 interatomic distance is longer in **2**, 2.257(4) Å, than in **3**, 2.218(4) Å, and the H200–M1–H300 bond angle is narrower in **2**, 62(2)°, than in **3**, 70(3)°. The

experimental bond lengths and angles associated with the Rh1–H200–B1 and Rh1–H300–B1 interactions of compound **2** compare rather well with those reported for equivalent interactions in compounds **A**–**C** (Figure 2).[4c,11a,11b]

As the small differences in the values of the XRD-determined interatomic distances and angles that reflect the asymmetry of the M1–H200–B1 and M1–H300–B1 interactions in **2** and **3** are close to the experimental error and may also be due to packing effects in the solid state, we decided to optimize by DFT methods, without symmetry restrictions, the molecular structures of these compounds in order to see whether the different M1–H200–B1 and M1–H300–B1 interactions observed in the solid state are maintained in the gas phase. Interestingly, the DFT-optimized structures reflected the asymmetry suggested by the XRD structures. Therefore, the differences suggested by XRD between the M1–H200–B1 and M1–H300–B1 interactions within molecules of **2** and **3** have an intrinsic thermodynamic origin at the molecular level (they lead to the most stable molecular structure) and, therefore, are not due to experimental errors or packing effects.

Aiming at getting an insight into the M1–H200–B1 and M1–H300–B1 interactions in **2** and **3**, the electron density associated to the bonding within these molecules was theoretically studied under the perspective of the QTAIM.[15] A selection of the obtained results is graphically presented in Figure 4, while Table 2 contains the values of important topological parameters associated to the bond critical points (*bcp*'s) of selected bonds. In Figure 4, it can be clearly observed that the ring critical point (*rcp*) associated to the MH_2B ring is closer to H300 than to H200 and that this fact is more prominent in the iridium complex **3** than in the rhodium complex **2**.

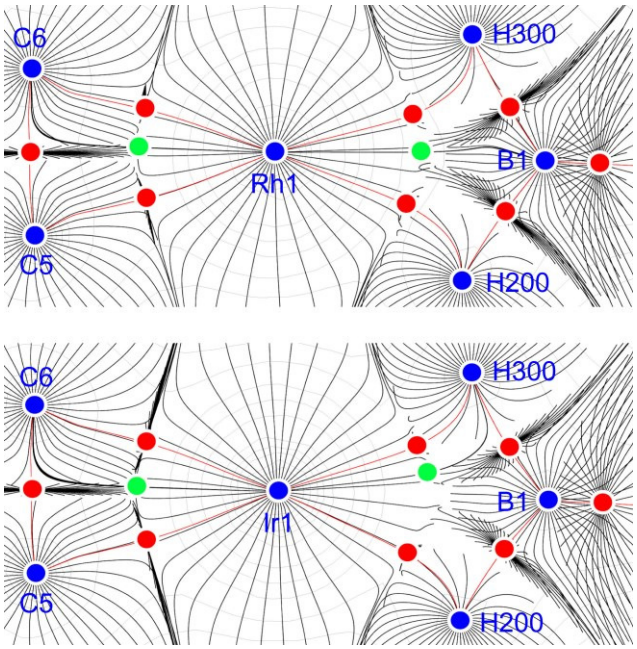

Figure 4. Gradient trajectories mapped on total electron density plots (contour levels at 0.1 e Å^{-3}) in the equatorial planes of compounds **2** (top) and **3** (bottom), showing the atomic basins, stationary points (blue circles), bond paths (red lines), bond critical points (red circles) and ring critical points (green circles).

Table 2. QTAIM Topological Parameters of Selected Bonds of Complexes 2 and 3

Complex	Bond	ρ_b (e Å^{-3})[a]	$\nabla^2\rho_b$ (e Å^{-5})[b]	ε_b[c]
2	Rh1–C[d]	0.677	4.933	0.689
	Rh1–N2	0.662	9.652	0.174
	Rh1–H200	0.521	5.525	2.325
	Rh1–H300	0.516	5.067	3.229
	B1–H100	1.185	–7.500	0.082
	B1–H200	0.981	–4.511	0.246
	B1–H300	0.981	–4.385	0.247
3	Ir1–C[d]	0.748	4.809	0.490
	Ir1–N2	0.743	10.611	0.189
	Ir1–H200	0.601	6.210	1.745
	Ir1–H300	0.587	5.675	2.994
	B1–H100	1.197	–7.926	0.067
	B1–H200	0.948	–4.553	0.319
	B1–H300	0.953	–4.410	0.316

[a]Electron density at the *bcp*.

[b]Laplacian of the electron density at the *bcp*.

[c]Ellipticity at the bcp.

[d]Average values.

There are two limiting forms for the interaction of a metal atom M with a B–H bond, namely, the terminal sigma coordination ($\kappa^1 H$), in which the BH fragment is attached to the metal through only the H atom, and the agostic-type coordination ($\kappa^2 H,B$), in which the metal is bonded to both B and H atoms. Interestingly, it has been recently reported that terminal sigma and agostic-type Rh–HB interactions have similar electron density at the Rh–H *bcp* (ρ_b) and similar Laplacian of the electron density at the Rh–H *bcp* ($\nabla^2\rho_b$), but different ellipticity at the Rh–H *bcp* (ε_b), that of the terminal sigma coordination being considerably smaller than that of the agostic-type coordination.[16] The only previous work that reports QTAIM data for Ir–HB interactions refers only to agostic-type B–H complexes.[17] In the case of compounds **2** and **3**, Table 2 shows that the ellipticities at the *bcp*'s of the M1–H200 bonds are clearly smaller than those of the M1–H300 bonds and that the difference is greater for the iridium complex **3** than for the rhodium complex **2**.

In addition, although the absence of an M–B *bcp* confirms a lack of an M–B bond, non negligible δ(MB) delocalization indexes were computed for both complexes, δ(Rh1B1) = 0.168, δ(Ir1B1) = 0.204. The delocalization index is an integral parameter (not associated to a *bcp*) that estimates the number of electron pairs delocalized between two atoms.[18] Therefore, there exists a weak interaction between M and B in compounds **2** and **3**, weaker in **2** than in **3**, which is not strong enough to be recognized as a bond by the QTAIM.

Accordingly, although the interaction of the two B–H groups of the H200–B1–H300 fragment of compounds **2** and **3** with their M atom has to be less agostic-type than terminal sigma B–H bond coordination (the QTAIM studies have found no bond between the M and the B atoms), (a) the asymmetry of the bond distances and angles associated to the M1–H200–B1 and M1–H300–B1 interactions, (b) the off-axis location of their associated *rcp*, which is closer to H300 than to H200, and (c) the greater values of the ellipticity at the *bcp* of the M–H300 bond than those of the M–H200 bonds, clearly confirm that the interaction of the B1–H300 bond with the M atom has a greater component of agostic-type B–H bond coordination than that of the B1–H200 bond. The numerical data also confirm that this difference is more pronounced for the iridium complex **3** than for the rhodium complex **2**.

In an attempt to get more insights into the nature of the asymmetry of the M1–H200–B1 and M1–H300–B1 interactions in **2** and **3**, we performed Natural Bond Orbital (NBO) calculations (Supporting Information).[19] While small metal contributions to the bonding orbitals responsible for the two M–H–B 3-centre-2-electron interactions (< 12 %) and small M–H Wiberg bond indices (0.17 for **2**

and 0.22 for **3**) confirmed that the M–H interactions are weak, these data proved to be unable to differentiate the M1–H200–B1 and M1–H300–B1 interactions.

Most probably, the coordination asymmetry of BH_2 fragment in complexes **2** and **3** is a consequence of the very narrow bite angle of the BH_2 fragment (62º in **2** and 70º in **3**), since a symmetric coordination of this fragment as a chelate to two equatorial sites of a trigonal bipyramidal metal complex (the ideal coordination angle is 120º) would imply either unacceptably short M–HB distances or smaller overlaps between the metal orbitals and the orbitals of the H_2B fragment (in comparison with those of the asymmetric coordination). In fact, and asymmetric chelating coordination of a BH_2 fragment has never been observed in square planar or octahedral complexes, in which the ideal coordination angle is 90º.

In solution, while the $^1H\{^{11}B\}$ NMR spectrum of compound **2** shows four very broad peaks for the cod vinylic and BH_3 protons at δ 4.54 (cod), 3.94 (cod), 3.19 (*H*BH_2Rh), and –1.65 (HB*H*$_2$Rh), that of compound **3** shows its cod vinylic protons as broad signals (δ 4.31 and 3.47), but its BH_3 protons as a sharp triplet at δ 5.02 (1 H, *H*BH_2Ir) and a sharp doublet at δ –3.34 (2 H, HB*H*$_2$Ir) with $J_{H\text{-}H}$ = 11.3 Hz. These data indicate that **2** and **3** are not rigid in solution at room temperature, but, while the cod ligands of **2** and **3** and the BH_3 group of **2** participate in fluxional processes at room temperature, the BH_3 group of **3** is rather rigid at this temperature. At 233 K, the $^1H\{^{11}B\}$ NMR spectrum of compound **2** shows the BH_3 protons as a double triplet at δ 3.26 and a double doublet at δ –1.63 with $J_{H\text{-}Rh}$ = 23.6 Hz and $J_{H\text{-}H}$ = 12.5 Hz. Therefore, the asymmetry of the M1–H200–B1 and M1–H300–B1 interactions indicated by the XRD and theoretical studies is not evident in solution.

Variable temperature (VT) $^1H\{^{11}B\}$ NMR studies on [$^2H_8$]-toluene solutions of compounds **2** (Figure 5) and **3** (Figure 6) indicate that all four cod vinyl protons are equivalent at high temperatures and the same occurs for the three protons of the BH_3 group (for the iridium complex **3**, it has not been possible to reach the temperature that makes equivalent its three BH_3 protons). Line-shape analyses of these spectra and their associated Eyring plots (Supporting Information) yielded the activation parameters of these fluxional processes (Table 3). The small and negative values of the activation entropies are consistent with intramolecular processes. Similar dynamic processes have been observed in solution by ^1H NMR for the BH_3 groups of the related rhodium(I) complexes **B**[11a] and **C**[11c] (Figure 2); however, these reports do not mention any fluxional process involving the cod ligand.

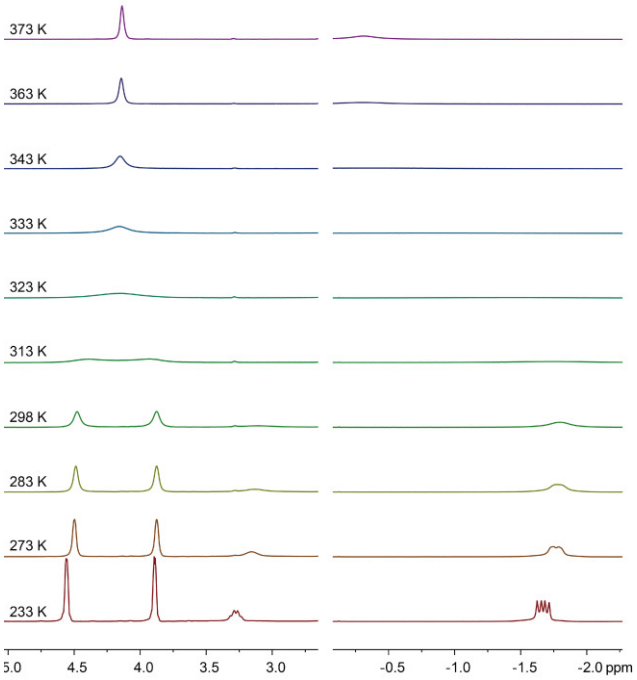

Figure 5. Representative regions of the $^{1}H\{^{11}B\}$ NMR spectra of complex **2** in [$^{2}H_{8}$]-toluene at various temperatures.

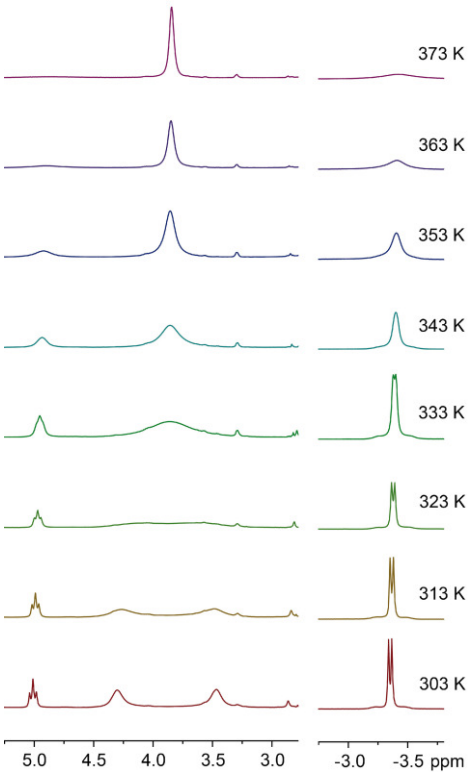

Figure 6. Representative regions of the $^{1}H\{^{11}B\}$ NMR spectra of complex **3** in [$^{2}H_{8}$]-toluene at various temperatures.

Table 3. Experimental Activation Parameters for the Fluxional Processes Occurring in Complexes 2 and 3[a]

Complex	Process	$\Delta H^{\ddagger}$	$\Delta S^{\ddagger}$	$\Delta G^{\ddagger}_{298}$
2	cod rotation	14.1	–1.6	14.6
3	cod rotation	13.7	–3.5	14.7
2	BH_3 rotation	12.6	–4.1	13.8
3	BH_3 rotation	15.6	–4.5	16.9

[a]Measured in [$^2H_8$]-toluene solutions; $\Delta H^{\ddagger}$ and $\Delta G^{\ddagger}$ in kcal mol^{-1}; $\Delta S^{\ddagger}$ in cal K^{-1} mol^{-1}.

The VT $^1H\{^{11}B\}$ NMR data suggest that, in solution, two fluxional processes are occurring concomitantly in **2** and **3**, namely, a rotation of the cod ligand that makes equivalent its two alkene fragments and a rotation of the BH_3 group about the B–N bond that exchanges the three B–H bonds. This suggestion was probed with DFT calculations (Figure 7).

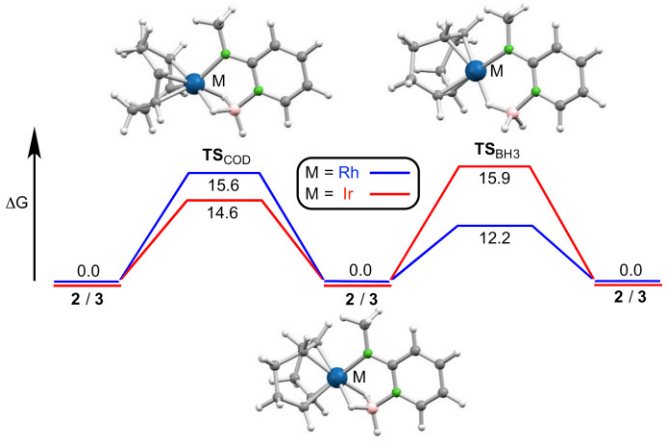

Figure 7. Calculated (DFT) mechanisms for the rotation of the cod ligand and the BH_3 fragment in complexes **2** and **3**. Gibbs energies (kcal mol^{-1}), relative to that of **2** or **3**, have been computed in toluene solution (CPCM solvation model).

In the case of the cod rotation, the exchange mechanism is an elemental process whose transition state (**TS**$_{COD}$) has a distorted square pyramidal coordination geometry with the cod olefinic fragments and the H atoms of the chelating H_2B fragment in the basal corners of the pyramid. The computed free energies of activation, 15.6 kcal mol^{-1} for **2** and 14.6 kcal mol^{-1} for **3**, compare well with the experimental values (Table 3) and are consistent with facile room temperature exchange. The activation barriers of these intramolecular rearrangements are low probably because they occur in pentacoordinate complexes, in which a change from square pyramidal to trigonal bipyramidal coordination is generally very easy.[20]

An elemental process is also responsible for the rotation of the BH_3 group. Its transition state ($\mathbf{TS}_{BH3}$) is a symmetric square planar species having the BH_3 group attached to the metal atom through only one H atom. In this case, the computed free energies of activation, 12.2 kcal mol^{-1} for **2** and 16.9 kcal mol^{-1} for **3**, also compare well with the experimental ones (Table 3) and clearly account for the experimental observation that the BH_3 group of the iridium complex starts to rotate at a higher temperature than that of the rhodium complex. The fact that the square planar transition state ($\mathbf{TS}_{BH3}$) of the iridium process is less stable than that of the rhodium process follows the general trend that iridium(I) complexes are more predisposed to be pentacoordinate than rhodium(I) complexes.[21]

The room temperature $^{11}B\{^1H\}$ NMR spectra of **2** and **3** are broad singlets centered at δ –10.0 and 0.6, respectively. Interestingly, the spectra of **2** shows no ^{11}B–^{103}Rh coupling. These signals split to a quartet ($J_{H\text{-}11B}$ = 87.4 Hz) and to a double triplet ($J_{H\text{-}11B}$ = 127 and 67 Hz), respectively, in the corresponding ^1H-coupled ^{11}B NMR spectra, confirming the fluxionality of the BH_3 group of complex **2** and a greater rigidity of the BH_3 group of complex **3** at room temperature.

CONCLUDING REMARKS

The reactions of $[M_2(\mu\text{-}Cl)_2(cod)_2]$ (M = Rh, Ir) with $K[mapyBH_3]$ lead to the trigonal bipyramidal complexes $[M(\kappa^3\textit{N,H,H}\text{-}mapyBH_3)(cod)]$ (M = Rh (**2**), Ir (**3**)), which contain a novel anionic tripod ligand coordinated to the metal atom through the amido N atom and through two H atoms of the BH_3 group.

XRD and QTAIM studies have revealed that the structural and electronic characteristics of the two M–H–B interactions of each complex are appreciably different within each complex, the difference being greater in **3** than in **2**. In fact, while both 3c–2e BH–M interactions are more $\kappa^1\textit{H}$ (terminal sigma coordination of the B–H bond) than $\kappa^2\textit{H,B}$ (agostic-type coordination of the B–H bond), one BH–M interaction is more agostic than the other and this difference is more marked in the iridium complex than in the rhodium one. The asymmetry of the MH_2B fragment of **2** and **3** has an intrinsic thermodynamic origin at the molecular level (it is not due to packing effects in the solid state), since DFT calculations have demonstrated that the most stable structures of these complexes are asymmetric in the gas phase. Most probably, this asymmetry is a consequence of the very narrow bite angle of the BH_2 fragment (62º in **2** and 70º in **3**), since a symmetric coordination of this fragment as a chelate to two equatorial sites of a trigonal bipyramidal metal complex (the ideal coordination angle is 120º) would imply either unacceptably short M–HB distances or smaller overlaps between the metal orbitals

and the orbitals of the H_2B fragment in comparison with the orbital overlaps of the asymmetric structure.

In solution, both complexes are fluxional at room temperature and above. VT-NMR and DFT studies have determined that the cod ligand rotates interchanging its two alkene fragments and that the BH_3 group equilibrates its three B–H bonds rotating about the B–N bond. While the cod rotation proceeds through a square pyramidal transition state and has a similar activation energy in **2** and **3**, the barrier to the BH_3 group rotation is higher in the iridium complex than in the rhodium one because it takes place through a square planar transition state and iridium(I) complexes are more predisposed to be pentacoordinate than rhodium(I) complexes.

EXPERIMENTAL SECTION

General Procedures. Solvents were dried over appropriate desiccating reagents and were distilled under argon before use. All reactions, manipulations, and chromatographic separations were carried out under argon, using dry box and/or Schlenk-vacuum line techniques. The reaction products were vacuum-dried for several hours prior to being weighted and analyzed. The dimers $[M_2(\mu\text{-}Cl)_2(cod)_2]$ (M = Rh,[22] Ir[23]) were prepared following published procedures. All remaining reagents were purchased from commercial sources. NMR spectra were run on a Bruker NAV-400 instrument, using as standards a residual protic solvent resonance for ^1H [$\delta(C_6\mathit{H}D_5)$ = 7.16 ppm; $\delta(C_6D_5CD_2\mathit{H})$ = 2.08 ppm], a solvent resonance for ^{13}C [$\delta(\mathit{C}_6D_6)$ = 128.10 ppm; $\delta(C_6D_5\mathit{C}D_3)$ = 20.43 ppm], and external $F_3B{\cdot}OEt_2$ for ^{11}B [δ = 0.00 ppm]. Line-shape analyses of the VT-NMR spectra were performed with DNMR3[24] within the SPINWORKS package.[25] Elemental analyses were obtained with a Perkin-Elmer 2400 microanalyzer. HRMS were obtained with a Bruker Impact II mass spectrometer operating in the ESI-Q-ToF positive mode.

HmapyBH$_3$ (1): A THF solution of BH_3 (1.2 mL, 1 M, 1.2 mmol) was added to a solution of 2-methylaminopyridine (102 μL, 1.0 mmol) in toluene (1.5 mL) at –78 ºC. The initial colorless solution changed to light yellow. After stirring at –78 ºC for 1 h, the solvent was removed under reduced pressure at room temperature to give compound **1** as a white solid that was washed with hexane (2 x 5 mL) and dried *in vacuo* (110 mg, 91 %). Anal. (%) Calcd for $C_6H_{11}BN_2$ (M_W = 121.9762 amu): C, 59.08; H, 9.09; N, 22.97; found: C, 59.15; H, 9.16; N, 22.85. (+)-ESI HRMS: *m/z* 145.0910 $[M + Na]^+$. ^1H NMR (C_6D_6, 400.54 MHz, 298 K): δ 8.12 (d, $J_{H\text{-}H}$ = 7.2 Hz, 1 H, C*H*), 6.71 (t, $J_{H\text{-}H}$ = 7.2 Hz, 1 H, C*H*), 6.24 (s, br, 1 H, N*H*), 5.82 (t, $J_{H\text{-}H}$ = 7.2 Hz, 1 H, C*H*), 5.61 (d, $J_{H\text{-}H}$ = 7.2 Hz, 1 H, C*H*), 3.11 (br

q, $J_{H\text{-}11B}$ = 96 Hz, 3 H, BH_3), 1.90 (d, $J_{H\text{-}H}$ = 5.2 Hz, 3 H, *Me*) ppm; the broad quartet at 3.11 ppm collapses to a singlet in a $^1H\{^{11}B\}$ NMR spectrum. $^{13}C\{^1H\}$ NMR (C_6D_6, 100.72 MHz, 298 K): δ 155.5 (*C*), 146.3 (*C*H), 139.0 (*C*H), 110.7 (*C*H), 106.1 (*C*H), 28.0 (*Me*) ppm. ^{11}B NMR (C_6D_6, 128.51 MHz, 298 K): δ –16.1 (q, $J_{H\text{-}11B}$ = 96 Hz) ppm; this signal collapses to a singlet in a $^{11}B\{^1H\}$ NMR spectrum.

[Rh(κ^3*N*,*H*,*H*-mapyBH$_3$)(cod)] (2): A toluene solution of K[N(SiMe$_3$)$_2$] (0.4 mL, 0.5 M, 0.20 mmol) was added to a solution of HmapyBH$_3$ (19 mg, 0.16 mmol) in toluene (7 mL). The resulting yellow suspension was stirred at room temperature for 30 min. Solid [Rh$_2$(μ-Cl)$_2$(cod)$_2$] (39 mg, 0.08 mmol) was added and the mixture was stirred for 1 h. The initial yellow suspension changed to orange. The solid was filtered off and the filtrate was evaporated to dryness under reduced pressure. The resulting solid was washed with hexane (2 x 5 ml) and dried *in vacuo* to give **2** as a light orange solid (41 mg, 77 %). Anal. (%) Calcd for $C_{14}H_{22}BN_2Rh$ (M_W = 332.0549 amu): C, 50.64; H, 6.68; N, 8.44; found: C, 50.71; H, 6.73; N, 8.41. (+)-ESI HRMS: *m/z* 333.0993 $[M + H]^+$. ^1H NMR (C_6D_6, 400.54 MHz, 298 K): δ 7.73 (d, $J_{H\text{-}H}$ = 7.2 Hz, C*H* of mapy), 6.74 (t, $J_{H\text{-}H}$ = 7.2 Hz, C*H* of mapy), 6.25 (d, $J_{H\text{-}H}$ = 7.2 Hz, C*H* of mapy), 5.75 (t, $J_{H\text{-}H}$ = 7.2 Hz, C*H* of mapy), 4.54 (s, br, 2 H, 2 C*H* of cod), 3.94 (s, br, 2 H, 2 C*H* of cod), 3.19 (br, *H*BH$_2$), 2.47 (s, 3 H, *Me*), 2.74–1.59 (m, 8 H, 4 CH_2 of cod), –1.65 (s, vbr, 2 H, HBH_2) ppm; the very broad signal at –1.65 ppm slightly sharpens in a $^1H\{^{11}B\}$ NMR spectrum. $^{13}C\{^1H\}$ NMR (C_6D_6, 100.72 MHz. 298 K): δ 162.6 (*C* of mapy), 143.3 (*C*H of mapy), 134.8 (*C*H of mapy), 109.1 (*C*H of mapy), 105.9 (*C*H of mapy), 75.1 (2 *C*H of cod), 72.1 (2 *C*H of cod), 34.9 (*Me*), 31.9 (2 *C*H_2 of cod), 30.2 (2 *C*H_2 of cod) ppm. ^{11}B NMR (C_6D_6, 128.51 MHz, 298 K): δ –10.0 (q, $J_{H\text{-}11B}$ = 87.4 Hz, *B*H$_3$) ppm; this signal collapses to a singlet in a $^{11}B\{^1H\}$ NMR spectrum.

[Ir(κ^3*N*,*H*,*H*-mapyBH$_3$)(cod)] (3): A toluene solution of K[N(SiMe$_3$)$_2$] (0.2 mL, 0.5 M, 0.10 mmol) was added to a solution of HmapyBH$_3$ (12 mg, 0.10 mmol) in toluene (5 mL). The resulting yellow suspension was stirred at room temperature for 30 min. [Ir$_2$(μ-Cl)$_2$(cod)$_2$] (33 mg. 0.05 mmol) was added and the mixture was stirred for 1 h. The initial yellow suspension changed to light brown. The solid was filtered off and the filtrate was evaporated to dryness under reduced pressure. The resulting solid was washed with hexane (2 x 5 ml) and dried *in vacuo* to give **2** as a light brown solid (37 mg, 88 %). Anal. (%) Calcd for $C_{14}H_{22}BIrN_2$ (M_W = 421.3655 amu): C, 39.91; H, 5.26; N, 6.64; found: C, 39.96; H, 5.31; N, 6.58. (+)-ESI HRMS: *m/z* 421.1416 $[M]^+$. ^1H NMR ($C_6D_5CD_3$, 400.54 MHz, 298 K): δ 7.64 (d, $J_{H\text{-}H}$ = 7.1 Hz, 1 H, C*H*), 6.69 (t, $J_{H\text{-}H}$ = 7.1 Hz, 1 H, C*H*), 6.28 (d, $J_{H\text{-}H}$ = 7.1 Hz, 1 H, C*H*), 5.77 (t, $J_{H\text{-}H}$ = 7.1 Hz, 1 H, C*H*), 5.02 (q, br, $J_{H\text{-}11B}$ = 127 Hz, 1 H, *H*BH$_2$), 4.31 (s, br, 2

H, 2 C*H* of cod), 3.47 (s, br, 2 H, 2 C*H* of cod), 2.61 (s, 3 H, *Me*), 2.53–1.78 (m, 8 H, 4 CH_2 of cod), –3.34 (q, br, $J_{H\text{-}11B}$ = 67 Hz, 2 H, HBH_2) ppm; the broad quartets at 5.02 and –3.34 ppm are transformed into a triplet ($J_{H\text{-}H}$ = 11.3 Hz) and a doublet ($J_{H\text{-}H}$ = 11.3 Hz), respectively, in a $^{1}H\{^{11}B\}$ NMR spectrum. $^{13}C\{^{1}H\}$ NMR ($C_6D_5CD_3$, 100.72 MHz, 298 K): δ 164.1 (*C* of mapy), 143.1 (*C*H of mapy), 135.1 (*C*H of mapy), 109.4 (*C*H of mapy), 106.7 (*C*H of mapy), 59.1 (2 *C*H of cod), 53.2 (2 *C*H of cod), 34.34 (*Me*), 32.9 (2 *C*H_2 of cod), 31.0 (2 *C*H_2 of cod) ppm. ^{11}B NMR ($C_6D_5CD_3$, 128.51 MHz, 298 K): δ 0.6 (dt, $J_{H\text{-}11B}$ = 127 and 67 Hz, *B*H_3); this signal collapses to a singlet in a $^{11}B\{^{1}H\}$ NMR spectrum.

X-Ray Diffraction Analyses: Crystals of **2** and **3** were analyzed by X-ray diffraction. A selection of crystal, measurement, and refinement data is given in the Supporting Information (Table S1). Diffraction data were collected on an Oxford Diffraction Xcalibur Onyx Nova single crystal diffractometer. Empirical absorption corrections were applied using the SCALE3 ABSPACK algorithm as implemented in CrysAlisPro RED.[26] The structures were solved using SIR-97.[27] Isotropic and full matrix anisotropic least square refinements were carried out using SHELXL.[28] All non-H atoms were refined anisotropically. The H atoms of **2** and those of the BH_3 moiety of **3** were located in their corresponding Fourier maps and were freely refined. The remaining H atoms of **3** were set in calculated positions and were refined riding on their parent atoms. The WINGX program system[29] was used throughout the structure determinations. The molecular plots were made with X-SEED.[30] CCDC deposition numbers: 1482288 (**2**), 1482289 (**3**).

QTAIM Studies: The structures of **2** and **3** were initially optimized with relativistic wavefunctions using the scalar ZORA hamiltonian, the PW91 density functional, and the all-electron relativistic QZ4P basis set for all atoms,[31] as implemented in the ADF2012 program package.[32] Subsequently, a fully relativistic four-component hamiltonian including spin-orbit terms in double-group symmetry and the hybrid B1PW91 density functional with QZ4P basis sets were used for single-point electronic structure calculations at the optimized geometries. The obtained ground-state electronic wavefunctions, which were found to be stable, were then utilized for the QTAIM calculations, which included both local and integral properties and were carried out with the AIMAll,[33] AIM2000,[34] and DGrid[35] programs. The accuracy of the local properties was 1.0×10^{-10} (from the gradient of the electron density at the *bcp*'s), whereas that of the integral properties was finally set at least at 1.0×10^{-4} (from the Laplacian of the integrated electron density).

NBO and Mechanistic Studies: For these studies, the DFT calculations were carried out using the wB97XD functional,[36] which includes the second generation of Grimme's dispersion interaction correction[37] as well as long-range interactions effects. This functional reproduces the local coordination geometry of transition metal compounds very well and it also corrects the systematic overestimation of non-bonded distances seen for all the density functionals not including estimates of dispersion. The Stuttgart-Dresden relativistic effective core potentials and the associated basis sets (SDD) were used for the Rh[38] and Ir[39] atoms. The basis set used for the remaining atoms was the cc-pVTZ.[40] All stationary points were fully optimized in gas phase and confirmed as energy minima or transition states by analytical calculation of frequencies. The electronic energies of the optimized structures were used to calculate the zero-point corrected energies and the enthalpic and entropic contributions via vibrational frequency calculations. Solvation free energies were obtained with the self-consistent reaction field (SCRF) for the standard continuum solvation model (CPCM),[41] by using the single-point solvation energy of the optimized structures and the thermodynamic correction from the gas phase calculations. All Gibbs energies were computed at 298.15 K and 1.0 atm. All calculations were carried out with the Gaussian09 package.[42]

ASSOCIATED CONTENT

Supporting Information. ^{1}H, ^{1}H{^{11}B}, ^{13}C{^{1}H}, ^{11}B, and ^{11}B{^{1}H} NMR spectra (Figures S1–S6); Line-shape analysis of the VT-NMR spectra (Figures S7–S14); ESI-HRMS data (Figure S15); Complementary figures obtained from the QTAIM studies (Figures S16–S18); Wiberg bond indices (Figure S19); Images of selected molecular orbitals (Figure S20); Crystal, acquisition, and refinement XRD data (Table S1); Comparison between experimental (XRD) and calculated (DFT) interatomic distances and angles in **2** and **3** (Tables S2 and S3); Complementary data obtained from the QTAIM studies (Tables S4–S6); Atomic coordinates of DFT-optimized structures in .xyz format; X-ray crystallographic data in .cif format. The Supporting Information is available free of charge on the ACS Publication website at DOI: 10.1021/cas.inorgchem.0000000.

AUTHOR INFORMATION

Corresponding Author

*E-mail (J. A. Cabeza): jac@uniovi.es.

Author Contributions

The manuscript was written through contributions of all authors. All authors have given approval to the final version of the manuscript.

Notes

The authors declare no competing financial interest.

ACKNOWLEDGMENTS

This work has been supported by grants from MINECO-FEDER (CTQ2013-40619-P, MAT2013-40950-R, and RYC-2012-10491) and Gobierno del Principado de Asturias (GRUPIN14-009 and GRUPIN14-060).

REFERENCES

(1) (a) Staubitz, A.; Robertson, A. P. M.; Manners, I. *Chem. Rev.* **2010**, *110*, 4079–4124. (b) Hamilton, C. W.; Baker, R. T.; Staubitz, A.; Manners, I. *Chem. Soc. Rev.* **2009**, *38*, 279–293. (c) Marder, T. B. *Angew. Chem. Int. Ed.* **2007**, *46*, 8116–8118. (d) Stephens, F. H.; Pons, V.; Baker, R. T. *Dalton Trans.* **2007**, 2613–2626.

(2) (a) Leitao, E. M.; Jurca, T.; Manners, I. *Nat. Chem*. **2013**, *5*, 817–829. (b) Clark, T. J.; Lee, K.; Manners, I. *Chem. Eur. J.* **2006**, *12*, 8634–8648. (c) Johnson, H. C.; Hooper, T. N.; Weller, A. S. *Top. Organomet. Chem*. **2015**, *49*, 153−220.

(3) Johnson, H. C.; Hooper, T. N.; Weller, A. S. in *Synthesis and Application of Organoboron Compounds*; vol. 49; Fernández, E., Whiting, A., Eds.; Springer International Publishing: New York City, NY, 2015, pp. 153–220.

(4) (a) Lunsford, A. M.; Blank, J. H.; Moncho, S.; Haas, S. C.; Muhammad, S.; Brohers, E. N.; Darensbourg, M. Y.; Bengali, A. A. *Inorg. Chem.* **2016***, 55*, 964–973. (b) Nako, A. E.; White, A. J. P.; Crimmin, M. R. *Dalton Trans.* **2015**, *44*, 12530–12534. (c) Dallanegra, R.; Chaplin, A. B.; Weller, A. S. *Angew. Chem. Int. Ed.* **2009**, *48*, 6875–6878.

(5) (a) Vance, J. R.; Schäfer, A.; Robertson, A. P. M.; Lee, K.; Turner, J.; Whittell, G. R.; Manners, I. *J. Am. Chem. Soc.* **2014**, *136*, 3048–3064. (b) Marziale, A. N.; Friedrich, A.; Klopsch, I.; Drees, M.; Celinski, V. R.; Schmedt auf der Günne, J.; Schneider, S. *J. Am. Chem. Soc.* 2013, *135*, 13342–13355. (c) Chaplin, A. B.; Weller, A. S. *Inorg. Chem.* **2010**, *49*, 1111–1121. (d) Stevens, C. J.; Dallanegra, R.;

Chaplin, A. B.; Weller, A. S.; Macgregor, S. A.; Ward, B.; McKay, D.; Alcaraz, G.; Sabo-Etienne, S. *Chem. Eur. J.* **2011***, 17*, 3011–3020. (e) Sewell, L. J.; Lloyd-Jones, G. C.; Weller, A. S. *J. Am. Chem. Soc.* **2012**, *134*, 3598–3610. (f) Johnson, H. C.; Leitao, E. M.; Whittell, G. R.; Manners, I.; Lloyd-Jones, G. C.; Weller, A. S. *J. Am. Chem. Soc.* **2014**, *136*, 9078–9093.

(6) (a) Wolstenholme, D. J.; Traboulsee, K. T.; Decken, A.; McGrady, G. S. *Organometallics* **2010**, *29*, 5769–5772. (b) Alcaraz, G.; Chaplin, A. B.; Stevens, C. J.; Clot, E.; Vendier, L.; Weller, A. S.; Sabo-Etienne, S. *Organometallics* **2010**, *29*, 5591–5595. (c) Vidovoc, D.; Addy, D. A.; Krämer, T.; McGrady, J.; Aldridge, S. *J. Am. Chem. Soc.* **2011**, *133*, 8494–8497. (d) Drover, M. W.; Bowes, E. G.; Schafer, L. L.; Love, J. A.; Weller, A. S. *Chem. Eur. J.* **2016**, *20*, 6793–6797. (e) Johnson, H. C.; Robertson, A. P. M.; Chaplin, A. B.; Sewell, L. J.; Thompson, A. L.; Haddow, M. F.; Manners, I.; Weller, A. S. *J. Am. Chem. Soc.* **2011**, *133*, 11076–11079.

(7) (a) Shimoi, M.; Nagai, S. I.; Ichikawa, M.; Kawano, Y.; Katoh, K.; Uruichi, M.; Ogino, H. *J. Am. Chem. Soc.* **1999**, *121*, 11704–11712. (b) Kubas, G. J. *Metal Dihydrogen and σ-Bond Complexes*; Springer: New York City, NY, 2001. (c) Alcaraz, G.; Sabo-Etienne, S. *Angew. Chem. Int. Ed.* **2010**, *49*, 7170–7179.

(8) Ramalakshmi, R.; Saha, K.; Roy, D. K.; Varghese, B.; Phukan, A. K.; Gosh, S. *Chem. Eur. J.* **2015**, *21*, 17191–17195.

(9) Huang, Y.; Stephan, D. W. *Organometallics* **1995**, *14*, 2835–2842.

(10) (a) van Dijkman, T. F.; de Brujin, H, M.; Siegler, M. A.; Bouwman, E. *Eur. J. Inorg. Chem.* **2015**, 5387–5394. (b) Dias, H. V. R.; Lu, H. L. *Inorg. Chem.* **2000**, *39*, 2246–2248. (c) Dias, H. V. R.; Lu, H. L.; Gorden, J. D.; Jin, W. *Inorg. Chem.* **1996**, *35*, 3935–3941.

(11) (a) Nguyen, D. H.; Lauréano, H.; Jugé, S.; Kalck, P.; Daran, J.-C.; Coppel, Y.; Urrutigoiti, M.; Gouygou, M. *Organometallics* **2009**, *28*, 6288–6292. (b) Ingleson, M.; Patmore, N. J.; Ruggiero, G. D.; Frost, C. G.; Mahon, M. F.; Willis, M. C.; Weller, A. S. *Organometallics* **2001**, *20*, 4434–4436. (c) Merle, N.; Frost, C. G.; Kociok-Köhn, G.; Willis, M. C.; Weller, A. S. *Eur. J. Inorg. Chem.* **2006**, 4068–4073. (d) Merle, N.; Kociok-Köhn, G.; Mahon, M. F.; Frost, C. G.; Ruggiero, G. D.; Weller, A. S. Willis, M. C. *Dalton Trans.* **2004**, 3883–3892. (e) Volkov, O.; Macías, R.; Rath, N. P.; Barton, L. *Inorg. Chem.* **2002**, *41*, 5837–5843.

(12) (a) Drover, M. W.; Schafer, L. L.; Love, J. A. *Angew. Chem. Int. Ed.* **2016**, *55*, 3181–3186. (b) Roy, D. K.; Borthakur, R.; Bhattacharyya, S.; Ramkumar, V.; Gosh, S. *J. Organomet. Chem.* **2015**, *799–800*, 132–137. (c) Rankin, M. A.; Hesp, K. D.; Schatte, G.; McDonald, R.; Stradiotto, M. *Dalton Trans*. **2009**, 4756–4765. (d) Stahl, T.; Müther, K.; Ohki, Y.; Tatsumi, K.; Oestreich, M. *J. Am. Chem. Soc.* **2013**, *135*, 10978 –10981. (e) Figueroa, J. S.; Melnick, J. G.; Parkin, G. *Inorg. Chem.* **2006**, *45*, 7056–7058. (f) Gloaguen, Y.; Alcaraz, G.; Pecharman, A.-F.; Clot, E.; Vendier, L.; Sabo-Etienne, S. *Angew. Chem. Int. Ed.* **2009**, *48*, 2964–2968. (g) Gloaguen, Y.; Alcaraz, G.; Petit, A. S.; Clot, E.; Coppel, Y.; Vendier, L.; Sabo-Etienne, S. *J. Am. Chem. Soc.* **2011**, *133*, 17232–17238. (h) Cassen, A.; Gloaguen, Y.; Vendier, L.; Duhayon, C.; Poblador-Bahamonde, A.; Raynaud, C.; Clot, E.; Alcaraz, G.; Sabo-Etienne, S. *Angew. Chem. Int. Ed.* **2014**, *53*, 7569–7573. (i) Ganguly, G.; Malakar, T.; Paul, A. *ACS Catal.* **2015**, *5*, 2754. (j) Lin, T.-P.; Peters, J. C. *J. Am. Chem. Soc.* **2014**, *136*, 13672–13683. (j) Drover, M. W. ; Bowes, E. G.; Schafer, L. L.; Love, J. A.; Weller, A. S. *Chem. Eur. J.* **2016**, *22*, 6793–6797. (k) Drover, M. W.; Johnson, H. C.; Schafer, L. L.; Love, J. A.; Weller, A. S. *Organometallics* **2015**, *34*, 3849–3856. (l) Merle, N.; Frost, C. G.; Kociok-Köhn, G.; Willis, M. C.; Weller, A. S. *J. Organomet. Chem.* **2005**, *690*, 2829–2834.

(13) (a) May, C. E.; Niedenzu, K. *Synth. React. Inorg. Met.-Org. Chem.* **1977**, *7*, 509–517. (b) Foret, C. J.; Chiusano, M. A.; O'Brien, J. O.; Martin, D. R. *J. Inorg. Nucl. Chem.* **1980**, *42*, 165–169.

(14) Housecroft, C. E.; Sharpe, A. G. *Inorganic Chemistry*; 2nd ed.; Prentice Hall: Harlow, UK, 2004.

(15) (a) Bader, R. F. W. *Atoms in Molecules, a Quantum Theory*; Clarendon Press: Oxford, UK, 1990. (b) Popelier, P. L. A. *Atoms in Molecules, an Introduction*; Prentice Hall: Harlow, UK, 2000. (c) *The Quantum Theory of Atoms in Molecules*; Matta, C. F.; Boyd, R. J., Eds.; Wiley-VCH: Weinheim, Germany, 2007.

(16) Kumar, A.; Beattie, N. A.; Pike, S. D.; MacGregor, S. A.; Weller, A. S. *Angew. Chem. Int. Ed.* **2016**, *55*, 6651–6656.

(17) Drover, M. W.; Bowes, e. G.; Schafer, L. L.; Love, J. A.; Weller, A. S. *Chem. Eur. J.* **2016**, *22*, 6793–6797.

(18) See, for example: (a) Gatti, C. *Z. Kristallogr.* **2005**, *220*, 339–457. (b) Macchi, P.; Sironi, A. *Coord. Chem. Rev.* **2003**, *238*, 383–412. (c) Farrugia, L. J.; Evans, C.; Senn, H. M.; Aänninen, M. M.; Sillanpää, R. *Organometallics* **2012**, *31*, 2559–2570. (d) Van der Maelen, J. F.; Cabeza, J. A. *Theor. Chem. Acc.* **2016**, *135*, 64. (e) Van der Maelen, J. F.; Cabeza, J. A. *Inorg. Chem.* **2012**, *51*, 7384–7391. (f) Van der Maelen, J. F.; García-Granda, S.; Cabeza, J. A. *Comput. Theor. Chem.* **2011**, *968*, 55–63. (g) Cabeza, J. A.; Van der Maelen, J. F.; García-Granda, S. *Organometallics* **2009**, *28*, 3666–3672.

(19) Glendening, E.; Badenhoop, J. K.; Reed, A. E.; Carpenter, J. E.; Bohmann, J. A.; Morales, C. M.; Landis, C. R.; Weinhold, F. *Natural Bond Orbital*; version 6.0; Theoretical Chemistry Institute, University of Wisconsin: Madison, WI, 2013.

(20) Shapley, J. R.; Osborn, J. A. *Acc. Chem. Res.* **1973**, *6*, 305–312.

(21) White, C. *Organometallic Compounds of Cobalt, Rhodium, and Iridium*; Springer: Berlin, Germany, 1998.

(22) Giordano, G.; Crabtree, R. H.; Heintz, R. M.; Forster, D.; Morris, D. E. *Inorg. Synth.* **1990**, *28*, 88–90.

(23) Herde, J. L.; Lambert, J. C.; Senoff, C. V.; Cushing, M. A. *Inorg. Synth.* **1974**, *15*, 18–20.

(24) Binsch, G.; Kleier, D. A. *DNMR3*; SERC NMR Program Library; Daresbury, UK, 1977. (b) Tattershall, B.W. *DNM3RUN and N3PLOT for Windows*; Newcastle University: Newcastle, UK, 2007.

(25) Marat, K. *SPINWORKS*; version 4.2.0; University of Manitoba: Winnipeg, Canada, 2015

(26) *CrysAlisPro RED*, version 1.171.37.35; Oxford Diffraction Ltd.: Oxford, UK, 2014.

(27) Altomare, A.; Burla, M. C.; Camalli, M.; Cascarano, G. L.; Giacovazzo, C.; Guagliardi, A., Moliterni, A. G. C.; Polidori, G.; Spagna, R. *J. Appl. Crystallogr.* **1999**, *32*, 115–119.

(28) *SHELXL-2014*: Sheldrick, G. M. *Acta Cryst.* **2008**, *A64*, 112–122.

(29) *WINGX*, version 1.80.05: Farrugia, L. J. *J. Appl. Crystallogr.* **1999**, *32*, 837–838.

(30) *X-SEED*: Barbour, L. J. *J. Supramol. Chem.* **2001**, *1*, 189–191.

(31) Van Lenthe, E; Baerends, E. J. *J. Comput. Chem.* **2003**, *24*, 1142–1156.

(32) Baerends, E. J. et al. *ADF2012*; revision 01d; SCM, Theoretical Chemistry, Vrije Universiteit: Amsterdam, The Netherlands, 2012.

(33) Keith, T. A. *AIMAll*; version 15.09.27; TK Gristmill Software: Overland Park, KS, 2015.

(34) *AIM2000*: Biegler-König, F.; Schönbohm, J. *J. Comput. Chem.* **2002**, *23*, 1489–1494.

(35) Kohout, M. *DGrid*; version 4.6; Max Planck Institute for Physical Chemistry of Solids: Dresden, Germany, 2011.

(36) Chai, J.-D.; Head-Gordon, M. *Phys. Chem. Chem. Phys.* **2008**, *10*, 6615–6620.

(37) (a) Ehrlich, S.; Moellmann, J.; Grimme, S. *Acc. Chem. Res.* **2013**, *46*, 916–926. (b) Grimme, S. *Comp. Mol. Sci.* **2011**, *1*, 211–228. (c) Schwabe, T.; Grimme, S. *Acc. Chem. Res.* **2008**, *41*, 569–579.

(38) Peterson, K.A.; Figgen, D.; Dolg, M.; Stoll, H. *J. Chem. Phys.* **2007**, *126*, 124101.

(39) Figgen, D.; Peterson, K. A.; Dolg, M.; Stoll, H. *J. Chem. Phys.* **2009**, *130*, 164108.

(40) Kendall, R. A.; Dunning Jr., T. H.; Harrison, R. J. *J. Chem. Phys.* **1992**, *96*, 6796-6806.

(41) (a) Barone, V.; Cossi, M. *J. Phys. Chem. A* **1998**, *102*, 1995–2001. (b) Cossi, M.; Rega, N.; Scalmani, G.; Barone, V. *J. Comput. Chem.* **2003**, *24*, 669–681.

(42) Frisch, M. J. et al. *Gaussian 09*; revision A.01; Gaussian, Inc.: Wallingford, CT, 2009.

ToC Synopsis and Graph

In trigonal bipyramidal rhodium(I) and iridium(I) complexes that contain 2-(methylamido)pyridine–borane as a tripod κ^3*N,H,H*-ligand, while both BH–M interactions are more terminal sigma (κ^1*H*) than agostic-type (κ^2*H,B*), one BH–M interaction is more agostic than the other and this difference is more marked in the iridium complex than in the rhodium one.